J. Phys. Chem. C 2024

https://doi.org/10.1021/acs.jpcc.4c07211

Modulating the Electronic Properties of Orthorhombic Mo_2C Surfaces with Strain and Defects: Insights from First-Principles Calculations

Sourabh Kumar,[1] Gokay Adabasi,[1] Mehmet Z. Baykara[1] and Ashlie Martini*,[1]

[1] *Department of Mechanical Engineering, University of California Merced, Merced, California 95343, United States*

Abstract

Mo_2C is an efficient and cost-effective catalyst for hydrogenation reactions that are crucial for chemical synthesis and renewable energy applications. In this study, we investigate the electronic and adsorption properties of orthorhombic Mo_2C (001) with three different surface terminations using density functional theory. By introducing Mo and C vacancies and substituting Mo with Ti, we evaluate the effect of defects on the electron localization function (ELF), projected density of states, and hydrogen adsorption behavior. The results show that Mo atom vacancies significantly disrupt the ELF distribution, while C atom vacancies and Ti substitution have little effect. Tensile or compressive strain applied to the surfaces modulates the ELF for surfaces with Mo defects but has little effect on systems with C vacancies or Ti substitutions. We also examine how defects and strain affect hydrogen adsorption on the Mo_2C surfaces to understand the potential effect on catalytic performance. The findings of this study highlight the importance of defect and strain conditions in the catalytic efficiency of orthorhombic Mo_2C

* Corresponding author. Email: amartini@ucmerced.edu

and offer valuable insight for designing strain- and defect-engineered catalysts with enhanced hydrogen adsorption and desorption properties, paving the way for more efficient and selective hydrogenation processes.

Introduction

Metal carbides are a class of compounds composed of carbon and metals, known for their exceptional hardness, high melting points, and significant resistance to wear and corrosion.[1–4] These materials are widely utilized in various industrial applications, including cutting tools, abrasives, and coatings, due to their robustness and durability.[5,6] Among the different types of metal carbides, tungsten carbide,[7,8] titanium carbide,[9,10] zirconium carbide[11] and molybdenum carbide are particularly noteworthy for their outstanding mechanical and catalytic properties.[12] The ability of these metal carbides to mimic the catalytic behavior of noble metals, particularly platinum, has made them a focal point in the search for alternative catalysts for various chemical processes.

Among metal carbides, molybdenum carbide (Mo_2C) stands out due to its exceptional catalytic properties,[13] especially in reactions like hydrogenation,[14] hydrogen evolution reaction (HER),[15–17] water-gas shift (WGS),[18,19] hydrodesulfurization,[20] (HDS) and hydrodeoxygenation[21] (HDO). Of particular importance is its role in hydrogenation, where the adsorption and activation of hydrogen molecules on the catalyst surface are critical for enabling efficient hydrogen transfer to substrates. The efficiency of hydrogenation catalysis is closely tied to the binding energy of hydrogen on the catalyst surface, which influences the adsorption, activation, and desorption processes essential for catalytic turnover.[22] Mo_2C has emerged as a particularly important catalyst for hydrogenation due to its ability to balance hydrogen adsorption and desorption efficiently, positioning it as a highly reliable and cost-effective choice for various hydrogenation applications, including CO_2 reduction,[14,23] olefin hydrogenation,[24] and selective hydrocarbon synthesis.[25] Additionally, the strong covalent bonds between Mo and C atoms contribute to good structural and thermal stability as well as high hardness such that Mo_2C is ideal for use in high-temperature and high-wear environments. The catalytic efficiency of Mo_2C, combined with its durability and stability, makes it an attractive choice for renewable energy technologies.[26]

Mo_2C can crystallize in several structural phases, with the two most common being orthorhombic and hexagonal close-packed. Here we focus on the orthorhombic phase of Mo_2C that exhibits distinct physical and chemical properties For example, experimental findings have highlighted the differences between hexagonal and orthorhombic structural stability caused by the concentration of carbon atoms[27] and the ordered/disordered distribution of carbon atoms at octahedral sites.[28,29] Studies have shown that the orthorhombic structure is beneficial for properties including catalytic activity,[30] mechanical strength,[31] and stability.[32] Orthorhombic Mo_2C with four different terminations, (001)-Mo-1, (001)-Mo-2, (001)-Mo-C, and (110)-Mo/C, was the-

oretically investigated previously.[33] Ab initio atomistic thermodynamic analysis showed that the (001)-Mo-C and (110)-Mo/C surfaces are the most stable. It was concluded that the presence of C atoms on the surface reduces reactivity, while surfaces with higher concentrations of Mo or metal atoms can promote hydrogenation reactions.[33]

In a combined experimental and computational study,[34] HDS reactions were analyzed with Ni_2P (001), orthorhombic Mo_2C (001), and polycrystalline MoC surfaces. The results showed that orthorhombic Mo_2C (001) had the highest reactivity. However, due to strong reactivity with the products, orthorhombic Mo_2C was found to be a less effective HDS catalyst than Ni_2P. This difference motivates the investigation of the atomic-scale mechanisms underlying the effect of surface electronic properties on the chemical reactivity, and thus catalytic properties. A recent computational study investigating the electrocatalytic mechanism of HER on Mo_2C, MoP, and Ni_2P surfaces revealed that the most effective catalytic sites are not necessarily those with the strongest adsorption.[35] This insight suggests that efficient hydrogen adsorption and desorption, rather than merely strong adsorption, is the key to enhancing catalytic activity. Moreover, calculations were used to analyze the effect of strain on the HER catalytic activity of the material. The study[35] reported that strain (e.g., 1% and 3% tensile strain for Mo_2C) enhances HER activity. The observed improvement in HER activity was explained in terms of adsorption energy (ΔE) and Gibbs free energy (ΔG) for hydrogen atoms on the surface. Previous studies focusing on different material surfaces, optimal adsorption energies, and strain suggest that fine-tuning these factors can lead to significant improvements in catalytic activity across various materials.[32,36]

Atomic level studies have shown that defects on the Mo_2C surface can alter its electronic properties.[37] Through Helmholtz free energy calculations and electron localization function (ELF) plots, a computational study provided an in-depth analysis of vacancy formation energies and defect sites.[38] The ELF plots showed that carbon vacancies exhibit a network of trapped electrons throughout the crystal, whereas molybdenum vacancies have significantly depleted electron density. Understanding these electronic structures in the unit cell provided critical insights for understanding the reactivity of the Mo_2C in catalytic processes.[38] However, a surface-level analysis can provide a better representation of vacancy-induced electronic changes compared to studies of a unit cell, and therefore enhance our understanding of how defects influence catalytic performance in practical applications.

A recent computational study aimed to investigate the role of defects on the catalytic behavior of γ-Mo_2C in an HER reaction.[39] The density functional theory (DFT) calculations revealed that doping and vacancy defects significantly improved the catalytic performance by shifting the

hydrogen adsorption free energy (ΔGH*) values closer to zero. Additionally, a negative linear relationship between the ΔGH* value and the d band center was found, suggesting that catalytic activity was modulated by tuning the d-band center and non-metal adsorption. This study[39] underscores the potential of modifying γ-Mo_2C through defects to tailor its catalytic properties. Such defect tailoring has not previously been explored at the atomic scale for orthorhombic Mo_2C.

Although the hexagonal and trigonal phases of Mo_2C have been thoroughly investigated via experiment and computational studies,[14,40–43] the role of defects (e.g., vacancies of Mo or C or substitution of foreign atoms) and strain (tensile and compressive) on the electronic properties of the surface of orthorhombic Mo_2C are yet to be explored. Thus, investigating how these factors affect the surface electronics of orthorhombic Mo_2C, particularly at the atomic level, is crucial for understanding and optimizing its catalytic properties.

In this study, we investigate how defects on the surface of orthorhombic Mo_2C and strain affect the electronic properties of the material. Motivated by representative conductive atomic force microscopy (C-AFM) images showing the effect of defects on surface electronics, we employ in silico methods, introducing various defects (vacancy and substitution) and performing strain calculations (uniaxial tensile and compression) on orthorhombic Mo_2C surfaces. As shown in Figure 1, we focus on Mo_2C (001) slab models with three different surface terminations: (001)-Mo-1, (001)-Mo-2, and (001)-Mo-C. The DFT-based results show how defects and strain on each type of orthorhombic Mo_2C surface affect the ELF. Moreover, hydrogen adsorption on surfaces with defects and/or subject to strain is analyzed. This analysis provides insights into how defects and strain affect catalytic efficiency and highlights the importance of tailoring orthorhombic Mo_2C for enhanced performance in catalytic applications.

Computational Details

Calculations were performed for three orthorhombic Mo_2C surfaces that will subsequently be referred to as different Types. Specifically, the (001)-Mo-1 surface is Type 1, the (001)-Mo-2 surface is Type 2, and the (001)-Mo-C is Type 3. All DFT calculations were performed using the Quantum ESPRESSO package.[44,45] The model systems were three layers of orthorhombic Mo_2C with an orthorhombic Bravais lattice. The 3×2×1.5 Mo_2C supercell utilized in this study was constructed from the optimized primitive unit cell with lattice parameter a = 4.734 Å, b = 6.063 Å, and c = 5.213 Å, which are in close agreement with experimental data (a = 4.732 Å, b = 6.037 Å, c = 5.204 Å).[46] Along the z-axis, a 12 Å vacuum was included both above and below

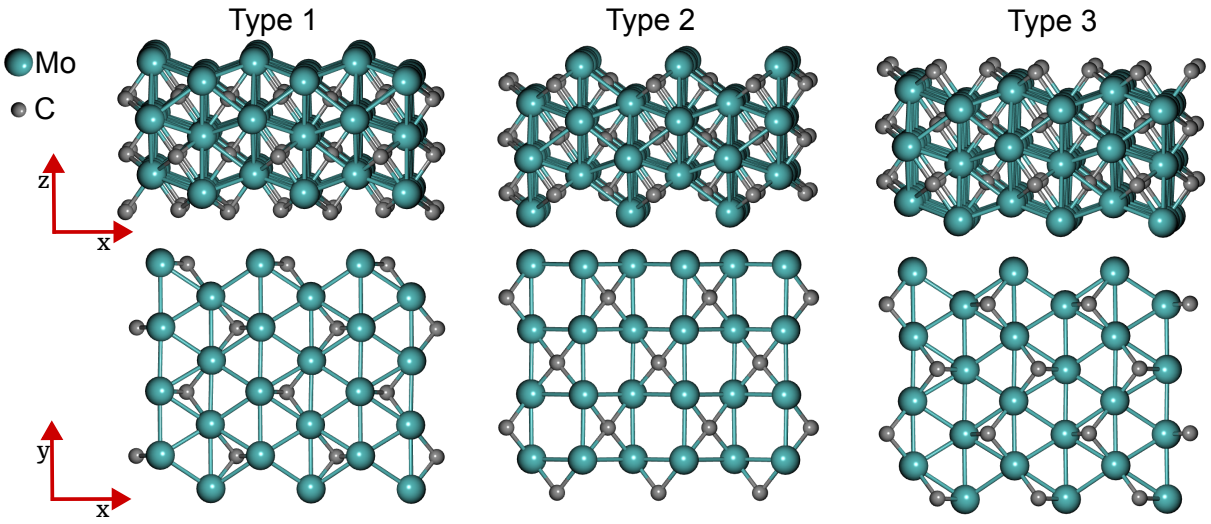

Figure 1: Orthorhombic Mo_2C (001) surfaces with different top layer atom structures used in the calculations: Type 1 (001)-Mo-1 – all Mo atoms, Type 2 (001)-Mo-2 – both Mo and C atoms on top, and Type 3 (001)-Mo-C – all C atoms on top. The first row images are side views (x, z axis) and the second row images are top views (with only the top layer of Mo and C atoms shown) of the system.

the material to mimic a slab conformation and avoid periodic interactions. The Perdew-Burke-Ernzerhof (PBE) functional, within the framework of the generalized gradient approximation (GGA), was employed to describe the exchange-correlation energy.[47] The plane-wave basis set was defined with a wavefunction cutoff energy of 665 eV. The self-consistent field (SCF) calculations achieved convergence with energy thresholds set to 10^{-5} eV for total energy calculations and 10^{-2} eV for geometry optimizations. The Monkhorst-Pack grid was centered at the Gamma point. Ionic positions were relaxed using the Broyden–Fletcher–Goldfarb–Shanno (BFGS) algorithm, allowing the system to find the local minimum energy configuration. The k-point sampling was carried out at the Gamma point, ensuring efficient and accurate integration over the Brillouin zone for this large supercell. Mechanical strain was introduced to the materials by distorting the crystal structure along the lattice constant a by changing the lattice parameter from its equilibrium value (a = 14.1856 Å) and performing optimization calculations using the variable cell relaxation. At each strain, the lengths of the simulation cell in the direction of the lattice constant a and c were fixed while the length in the direction of lattice constant b was allowed to change. This process permitted the relaxation of both lattice constants and atomic coordinates during the structural optimization. The computational parameters were chosen to ensure a balance between accuracy and computational cost, suitable for studying the impact of mechanical strain and defects on the electronic properties.

Experimental Details

The C-AFM images presented here were acquired on thin crystals of Mo_2C grown via chemical vapor deposition (CVD) on copper foils.[48] While the details of the synthesis can be found elsewhere, the overall process consists of the following main steps: (1) a Cu foil placed on top of a Mo foil was inserted into an atmospheric-pressure CVD furnace in a quartz crucible, (2) the samples were heated up to a temperature of 1090°C under a flow of N_2, H_2, and CH_4 gases, (3) the samples were rapidly cooled down out of the hot zone under N_2 and H_2 gas flow. Depending on growth times, this process resulted in thin Mo_2C crystals located on copper foils, with thicknesses ranging from a few tens to a few hundreds of nm and lateral sizes spanning several μm. A commercial AFM instrument was used for imaging (Asylum Research, Cypher VRS), which was performed under uncontrolled ambient conditions (temperatures of 30-35°C, measured inside the AFM instrument, and relative humidity levels of 30-40%). A conductive-diamond-coated probe (Nanosensors, CDT-NCHR) was utilized for imaging, with a normal spring constant of 68 N/m, calibrated by the Sader method.[49] Images were acquired at fast scan rates of 15.62 Hz, which were previously found to be conducive to high-resolution imaging.[50] No additional normal load was applied beyond the adhesive force at snap-in, which was typically on the order of 10 nN. During scans, the normal load and the bias voltage were kept constant, and the current between the sample and the probe was recorded as a function of lateral position, in the form of current maps.

Results and Discussion

Vacancy and Substitution Defects

Atomic-resolution, real-space images of Mo_2C surfaces obtained using C-AFM demonstrate that defects significantly affect surface electronics (Figure 2). In particular, Figure 2A shows an atomic-resolution image obtained on a pristine region of the Mo_2C surface, comprising bright spots (corresponding to high local conductivity) arranged in a hexagonal fashion. The symmetry and spacing of the bright spots indicate that they correspond to Mo atoms on a Type 1 surface (Figure 1). The image in Figure 2B, recorded on another region of the crystal surface, comprises the same atomic layout in the background as the pristine surface but also exhibits a larger bright feature, corresponding to a defect spanning several atomic sites that affects the local electronic landscape.

Motivated by the experimental observation that defects modulate the surface electronic

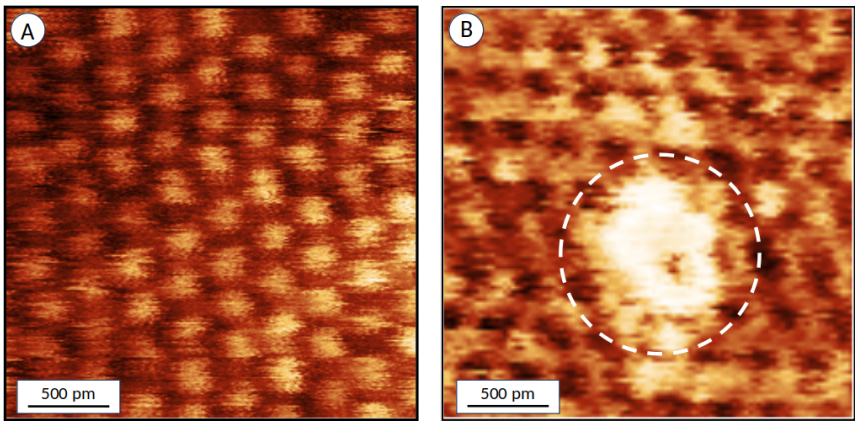

Figure 2: (A) An atomic resolution current map of the pristine Mo_2C surface (current range: 0.6 nA (dark) to 1.5 nA (bright), bias voltage: 5 mV). (B) An atomic resolution current map recorded on a region of the Mo_2C surface that contains a defect spanning multiple atomic sites, highlighted by the dashed circle (current range: 5.8 nA (dark) to 19.7 nA (bright), bias voltage: 5 mV).

landscape of Mo_2C significantly, we performed calculations to characterize the electronic properties of three different Mo_2C surfaces, introducing either a Mo or C vacancy in the top atomic layer of the material. The $Mo_{72}C_{36}$ supercell slab used in this study had a defect concentration of 1.39% for a single Mo vacancy and 2.78% for a single C vacancy. The resulting electronic property changes were then analyzed using ELF plots of the top lattice planes, as shown in Figure 3. The ELF, introduced by Becke and Edgecombe in 1990,[51] measures the spatial localization of electron pairs compared to a homogeneous electron gas. With values ranging from 0 to 1, ELF identifies regions of electron pairs localization: values near 1 indicate highly localized electron pairs, such as in covalent bonds, lone pairs, or core electrons, while values near 0.5 reflect delocalized electron pairs resembling a free electron gas, and values close to 0 represent electron pair deficient regions.[52] ELF plots provide a visual representation of this localization, revealing the electronic structure and bonding behavior in a system, including the effect of defects. We compared the ELF plots for the pristine surfaces (first row, Figure 3A-D), as well as surfaces with a static vacancy (second row, Figure 3E-H), and an optimized vacancy system (third row, Figure 3I-L). The static vacancy system refers to models of the defect-containing surfaces without structural optimization while the optimized vacancy system refers to models after complete relaxation. This comparison between the static and optimized vacancy systems enables isolation of the effect of local strain (atom displacement) caused by the defects. In all plots, the electron rich and deficient sites are represented by red and blue, respectively, with the green representing moderate ELF regions.

In the case of the Type 1 Mo_2C surface with an Mo vacancy (Figure 3E, I), the single Mo vacancy results in a blue region in the ELF, corresponding to the absence of electron pairs and related interactions near the missing atom's location, consistent with a disrupted bonding

environment. Optimization of this Mo-vacancy system further increases the size of the region with reduced ELF values, which can be directly attributed to the displacement of neighboring atoms caused by the lack of interactions with the missing atom due to the vacancy. Similarly, for the Mo_2C Type 2 surface with an Mo vacancy (Figure 3F, J), the ELF plots indicate a low-pairing probability at the vacancy site. However, compared to the Type 1 surface, the displacement of neighboring atoms due to the vacancy in the Type 2 surface is not significant. In the case of the Mo_2C Type 2 surface with a C vacancy (Figure 3G, K) and Mo_2C Type 3 surface with a C vacancy (Figure 3H, L), the ELF reveals regions of high values corresponding to electron pairs at the vacancy site, indicative of trapped electron pairs. The optimization of these sites does not lead to significant displacement of neighboring atoms, in contrast to the Type 1 surface with Mo vacancy. The ELF values of the optimized vacancy systems (both Mo and C vacancies), as shown in Figure 3, vary at the vacancy sites and are as follows: For Type 1, with a Mo vacancy, the ELF ranges from 0.01 at the Mo vacancy site to a maximum of 0.79 over the Mo atom. For Type 2, with a Mo vacancy, the ELF varies between a minimum of 0.01 at the Mo vacancy site and a maximum of 0.86 over the C atom, whereas for Type 2 with a C vacancy, the ELF ranges from 0.03 at the C vacancy site to a maximum of 0.83 over the C atom. For Type 3, with a C vacancy, the ELF has a minimum value of 0.48 at the C vacancy site and a maximum of 0.85 over the C atom. These ELF results benchmark and extend the findings from a previous study that reported similar electronic changes due to Mo and C atom vacancies with a unit cell system[38] and confirm the effect of vacancies on the electronic properties across surfaces terminated by different atoms (Mo and C) in the orthorhombic structure.

The substitution of Mo atoms with foreign atoms can significantly affect the electronic properties of Mo_2C.[39] Since the Mo vacancy on the Mo_2C Type 1 surface caused significant changes in the electronic structure (reduced the ELF values at the vacancy site) and the most significant atom displacement among the three surface types, we substituted an Mo atom on the Mo_2C surface (Type 1) with a Ti atom. As shown in Figure 4, the ELF plot (as viewed from different planes, i.e., 100, 010, and 001) shows that the substitution defect creates a minor perturbation in the surrounding electronic structure. The Ti atom site is surrounded by a blue color that indicates reduced pairing electrons with the neighboring atoms. These changes caused by the substitution of Mo atom with Ti atom indicate a modification in the local bonding environment and electronic structure, which could have implications for Mo_2C's electronic and catalytic properties.

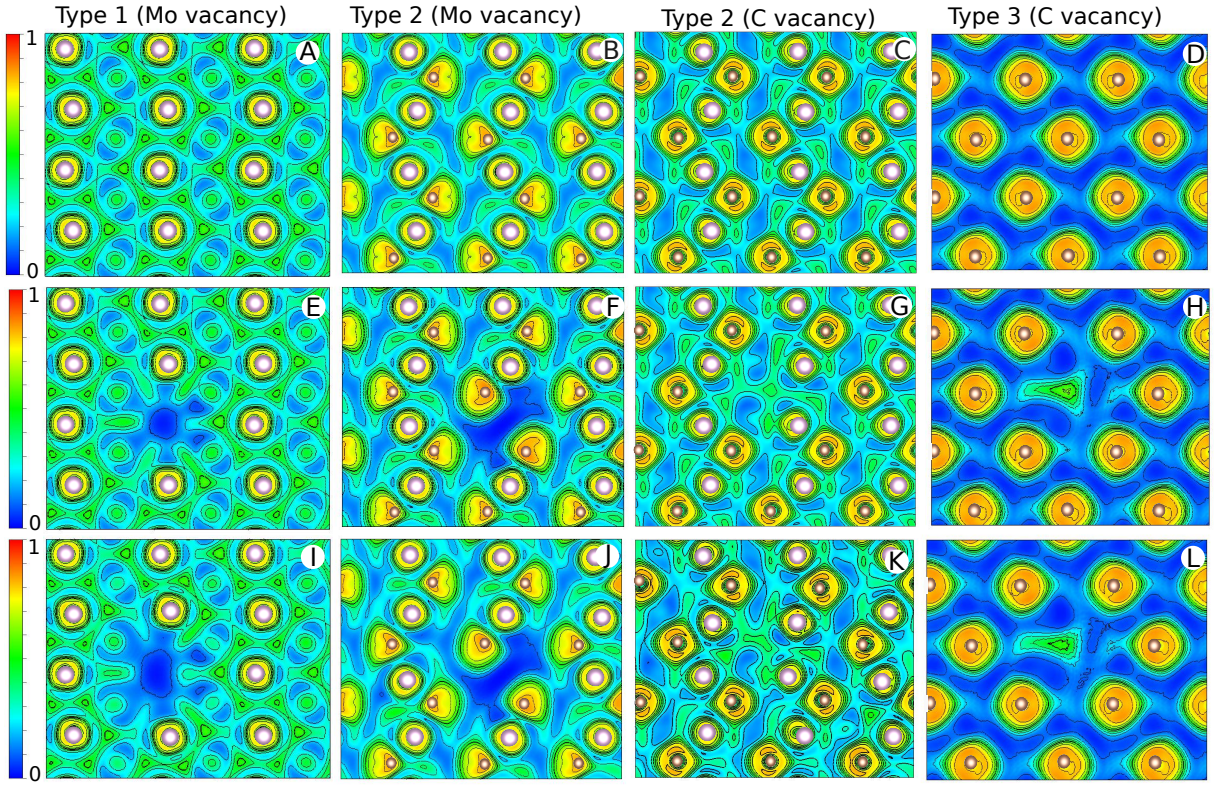

Figure 3: ELF plot for pristine (A, B, C and D), static vacancies (E, F, G and H), and optimized vacancies (H, I, J and K) on the orthorhombic Mo_2C surface. The plots represents the degree of electron localized in the x–y lattice plane.

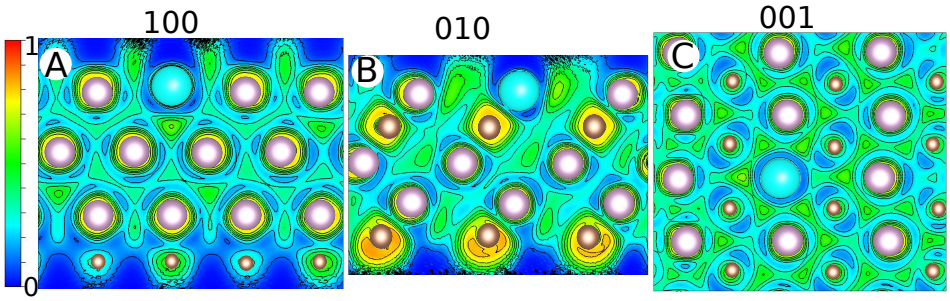

Figure 4: ELF plot for 100 (y–z plane), 010 (x–z lattice plane), and 001 (x–y lattice plane) for substitution of a single Mo atom with a Ti atom (light blue sphere) in the orthorhombic Mo_2C (Type 1) system.

External Strain

To analyze the strain-dependent electronic properties of the surface, we applied strain (tensile or compressive) to all three Mo_2C model systems both with and without vacancy defects. In this study, positive strain values (3%) represent tensile strain, while negative values (-3%) represent compressive strain. As shown in the ELF plots for the pristine system in Figure 5 (A, B for Type 1; C, D for Type 2 top Mo atoms plane; E, F for Type 2 top C atoms plane; G, H for Type 3), there is negligible difference in the electronic structure at 3% and -3% strains. The maximum tensile and compressive strain caused only slight changes in the ELF distribution. However, the introduction of strain and an atom vacancy led to significant changes, as shown in Figure

6 (A, B for Mo vacancy on Type 1; C, D for Mo vacancy on Type 2 top Mo atoms plane; E, F for C vacancy on Type 2 top C atoms plane; G, H for C vacancy on Type 3). For example, with 3% tensile strain, the size of the site where electron pairs were missing due to the vacancy (the blue region) in Type 1 system expands along both the a and b lattice directions due to the absence of bonded regions near the vacancy site. Similarly, with -3% compression, the missing electron pairs region due to the vacancy is smaller than that in the unstrained system. For Type 2, the Mo atom vacancy under both 3% and -3% strain exhibited the same effects in the ELF plot. In contrast, the C atom vacancies on Type 2 and Type 3 surfaces showed no significant changes in the ELF plot under strain, except for the presence of trapped electron pairs. These differences between the pristine and defective systems demonstrate the interrelated effects of vacancies and strain on surface electronic properties.

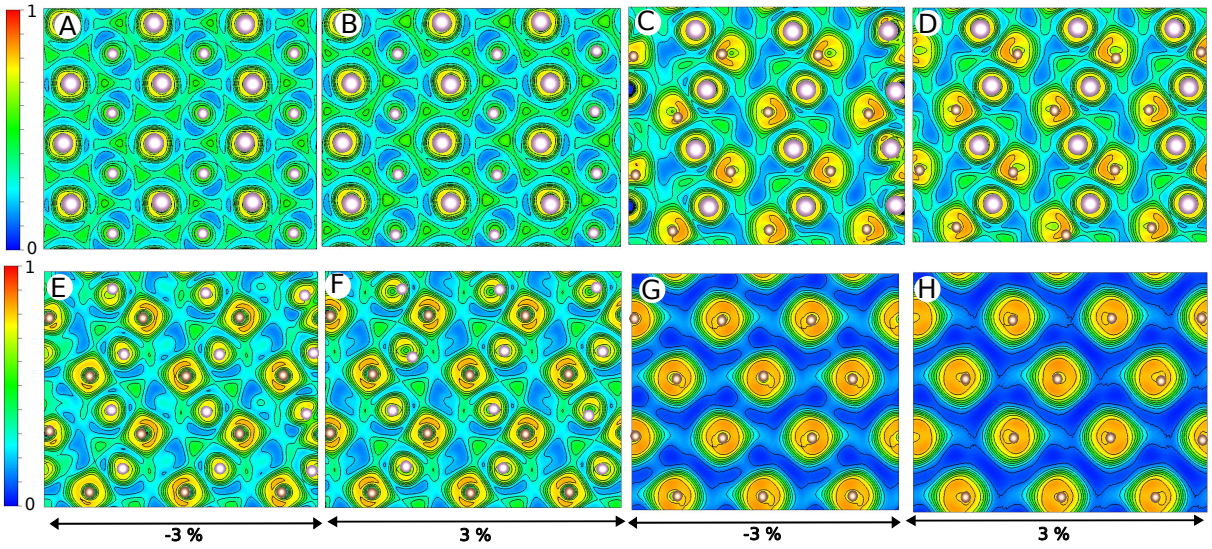

Figure 5: Effect of strain (compression and tension) on the ELF plots for pristine Type 1 (A and B), Type 2 Mo-terminated lattice plane (C and D), Type 2 C-terminated lattice plane (E and F) and Type 3 (G and H) system.

Unlike the effect of strain on the ELF plot of the Type 1 system with a Mo vacancy, substituting Mo with Ti in the Type 1 system did not result in significant changes in the electronic properties. For instance, both compressive (Figures 7A, C, E) and tensile (Figures 7B, D, F) strains caused no notable variations in the reduced ELF values in the vicinity of Ti atom. Therefore, applying strain to this system is unlikely to lead to significant changes in its catalytic properties.

We next investigated the effect of external strain on the projected density of states (PDOS) of the Mo_2C surface. This analysis was initially performed on the pristine Type 1 surface. The PDOS plots for Mo and C atoms under 3% tensile strain (Figure 8(A)), 0% strain (unstrained) (Figure 8(B)), and -3% compressive strain (Figure 8(C)) were examined. The fluctuations near the fermi energy level in the PDOS plots at different strain amounts indicate that tensile and

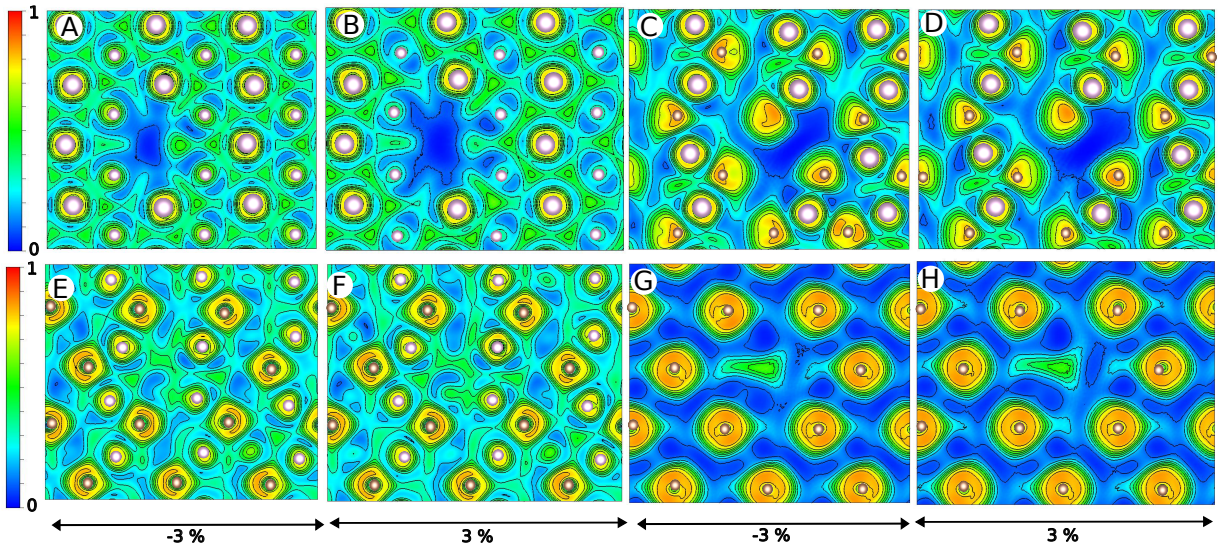

Figure 6: Effect of strain (compression and tension) on the ELF plots for Type 1 with Mo vacancy (A and B), Type 2 with Mo vacancy (C and D), Type 2 with C vacancy (E and F) and Type 3 with C vacancy (G and H).

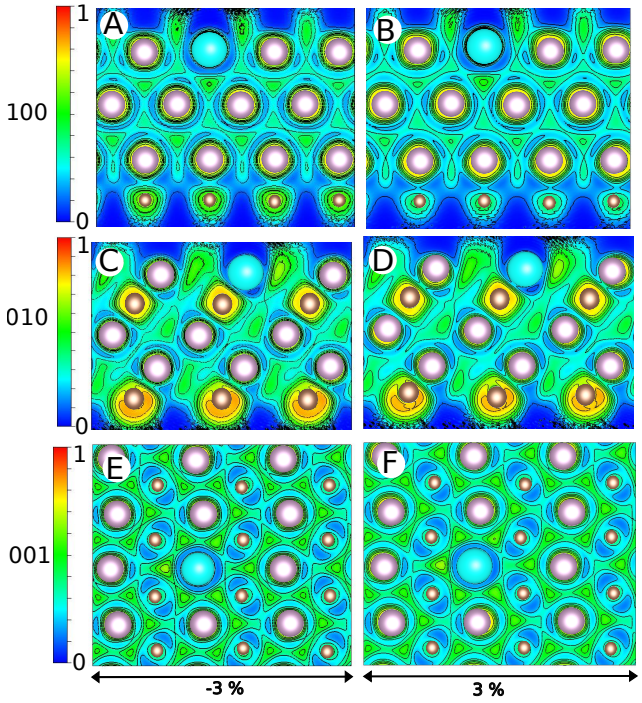

Figure 7: Effect of strain on the ELF plots in different planes (100, 010 and 001) for Mo-substituted Ti atom orthorhombic Mo2C (Type 1) system. Panels (A, C and E) show -3% compressive strain, while panels (B, D and F) show 3% tensile strain. The light blue sphere represents the Ti atom.

compressive strain cause significant shifts in the Mo-d-orbital, which could be due to the re-distributions in the electronic states of the Mo d-orbital. Under 3% tensile strain, the density of states for Mo and C atoms differ from those of the unstrained system, indicating changes in the electronic environment due to the applied strain. Similarly, -3% compressive strain results in distinct modifications in the PDOS, further confirming the strain-induced changes in the electronic structure. These modifications in the PDOS can be helpful to characterize the

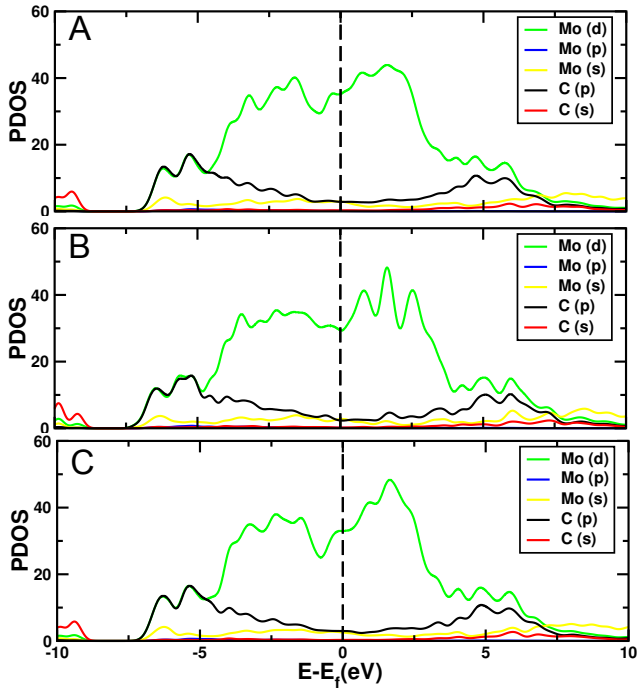

Figure 8: Effect of strain on the projected density of states (PDOS) for the orthorhombic Mo_2C (Type 1) system under 3% tensile strain (A), 0% unstrained (B), and -3% compressive strain (C).

electronic properties and chemical bonding present in both strained and unstrained systems. In all three cases (i.e. at 0%, 3%, and -3% strain) of the Type 1 system, the prominence of the Mo (d-orbitals) near the fermi energy level indicates a contribution to both covalent and metallic bonding between the Mo-C and Mo-Mo bonds in the system. These calculations were also performed for other surface types and the results in terms of changes in PDOS with respect to strain were not significantly different from those shown here for Type 1, so the other surface types were not explored further.

Surface Adsorption

The difference in adsorption energy between pristine and defective Mo_2C surfaces can depend on several factors, such as the type of defect, the nature of the adsorbate, and the specific adsorption site. Previous studies of hydrogen adsorption on Mo_2C surfaces have shown that Mo_2C exhibits strong catalytic properties, due to its ability to adsorb hydrogen effectively.[43] Moreover, the calculated surface potential of the Mo_2C varies significantly based on surface termination, with values of 4.82 eV for Type 1, 4.89 eV for Type 3, and 3.62 eV for Type 2 surfaces. These differences highlight the impact of termination on electron binding and surface properties, which can affect the adsorption properties. The pristine Mo_2C surface typically provides moderate adsorption energy, with the H atom favoring specific sites such as atop Mo, atop C, or at bridge sites between Mo-Mo and Mo-C atoms.[43,53,54] We performed hydrogen

adsorption energy calculations on the pristine as well as different types of defective and strained orthorhombic Mo_2C surfaces.

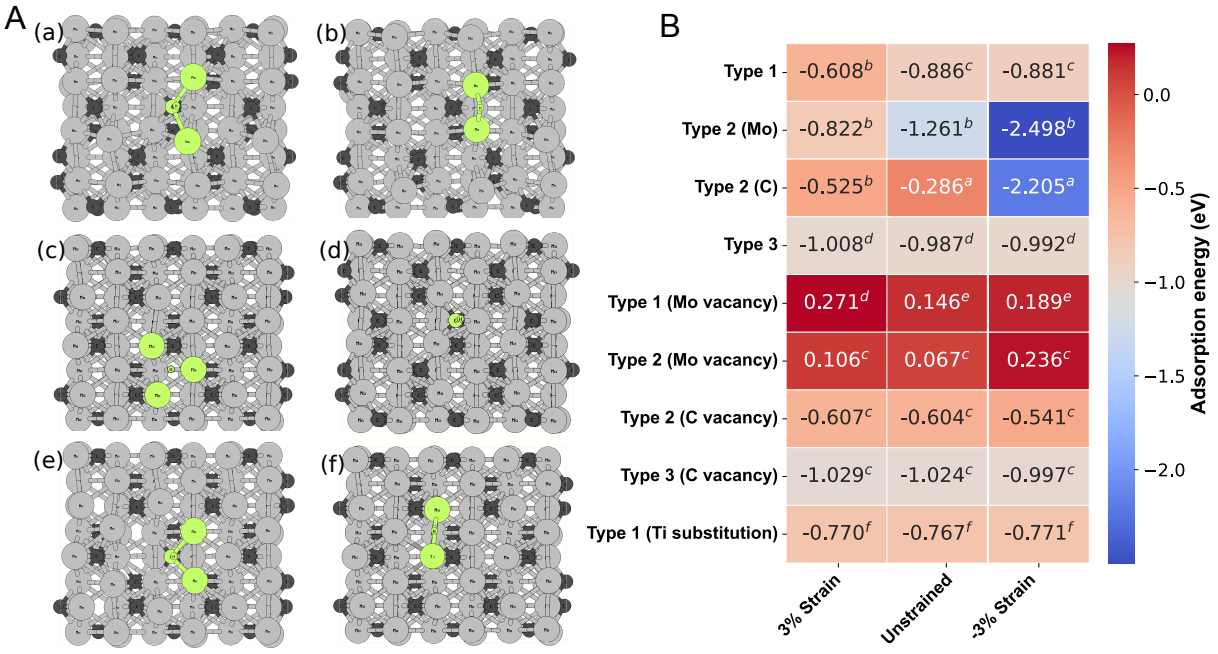

Figure 9: (A) Hydrogen adsorption sites: ^{a} Bridged between Mo and C atom. ^{b} Bridged between two Mo atoms. ^{c} Bridged between three Mo atoms. ^{d} atop C atom. ^{e} Bridged between one C and two Mo atoms. ^{f} Bridged between Mo and Ti atom. (B) Hydrogen adsorption energies on various orthorhombic Mo_2C surfaces.

As shown in Figure 9A and B, the presence of defects and application of strain influence the hydrogen adsorption sites and energies. Based on hydrogen adsorption optimization calculations, we found six different hydrogen adsorption configurations on all surfaces types. The hydrogen atoms adsorbed onto the Mo_2C surface by forming bonds with the d-orbitals of Mo and the p-orbitals of C can enable effective electron transfer and facilitate adsorption and desorption processes. When defects were introduced or strain applied, the hydrogen adsorption sites changed relative to the pristine system in some cases. Analysis of these hydrogen adsorption possibilities on various orthorhombic Mo_2C surfaces subject to defects and strain reveals several key findings.

Effect of Defects on Unstrained Systems: Pristine surfaces exhibit a range of adsorption energies that depend on the specific adsorption site and surface structure. In all unstrained pristine systems, hydrogen adsorption energies are negative, indicating favorable conditions for hydrogen binding. However, surface modifications, such as Mo vacancies, significantly alter these adsorption characteristics. For instance, Pristine Type 1 has an adsorption energy of -0.886 eV, while Pristine Type 2 (Mo) has a stronger adsorption energy of -1.261 eV. This suggests that these pristine surfaces are capable of effective hydrogen adsorption, which is essential for catalytic activity. Conversely, for Type 1 and Type 2 surfaces with Mo vacancies,

the hydrogen adsorption energy shifts to positive values (0.146 eV and 0.067 eV, respectively). This indicates that hydrogen adsorption becomes suboptimal and favors desorption. In the context of hydrogenation reactions, efficient performance requires a balance between effective adsorption of hydrogen onto the catalyst surface and its subsequent transfer to the substrate (desorption from the surface), ensuring smooth and complete conversion. The presence of Mo vacancies can create new active sites that enhance hydrogen adsorption while also modifying the electronic structure, potentially facilitating faster desorption rates. This balance between adsorption and desorption, influenced by vacancies, is essential for maximizing catalytic efficiency.

In terms of C vacancies, a Type 2 surface with a C vacancy has a negative adsorption energy of -0.604 eV, suggesting that C vacancies may enhance the ability of the surface to adsorb hydrogen without significantly hindering desorption. Similarly, Type 3 with C vacancy has a negative value of -1.024 eV, indicating that this surface configuration continues to support hydrogen binding effectively. These observations highlight that C vacancies can serve as beneficial sites for hydrogen adsorption. The change in the adsorption energies indicates that the vacancies affect the active sites relevant for effective hydrogen binding, rendering the surfaces less efficient for hydrogenation. In contrast, Type 2 with a C vacancy has a negative adsorption energy of -0.604 eV, indicating that C vacancies have a smaller impact on hydrogen adsorption strength than Mo vacancies. Similarly, Type 3 with a C vacancy shows only a slight reduction in adsorption energy to -1.024 eV, indicating that the presence of C vacancies does not significantly compromise the surface's catalytic potential. Moreover, the introduction of Ti atom substitution in Type 1 leads to a slight reduction in hydrogen adsorption energy from -0.886 eV to -0.767 eV. While the system remains favorable for adsorption, the reduced strength suggests a slight decrease in the hydrogen adsorption due to the foreign atom substitution.

Effect of Strain on Pristine Systems: Pristine systems generally offer stable hydrogen adsorption with less sensitivity to strain, especially for Type 1 and Type 3 surfaces. However, certain pristine surfaces (like Type 2, for hydrogen adsorption on either C or Mo atom) are highly responsive to strain, as the energies increase significantly from the unstrained to compressively strained system. In case of pristine Type 1, the system under 3% strain experiences a shift in adsorption energy from -0.886 eV to -0.608 eV, while pristine Type 2 transitions from -1.261 eV to -0.822 eV. While the adsorption remains negative in both cases, indicating some degree of favorability, the moderate increase in adsorption energies suggests that strain may slightly affect the interaction between hydrogen and the surface. However, for the pristine Type 2 system under 3% compressive strain, hydrogen adsorption increased significantly, with ad-

sorption energies changing from -1.261 eV to -2.498 eV for hydrogen adsorbed on the Mo atom and from -0.286 eV to -2.205 eV for hydrogen adsorbed on the C atom. These changes suggest that the compressive strain can significantly reduce the catalytic activity of the Type 2 system due to strong binding with hydrogen.

Effect of Strain on Defective Systems: The application of strain to the defective systems further modifies the adsorption behavior of hydrogen, providing insight into how mechanical properties can be tuned for improved catalytic performance. For example, the application of 3% strain results in increased adsorption energies for defective systems with Mo vacancies; Type 1 with Mo vacancy shows an energy of 0.271 eV, while Type 2 with Mo vacancy reaches 0.106 eV. Although these values remain positive, indicating weaker hydrogen adsorption, the application of strain does not sufficiently lower the adsorption energies to make the surface more favorable for hydrogen binding. Similarly, applying -3% strain leads to less favorable hydrogen adsorption, as seen in Type 1 with Mo vacancy and Type 2 with Mo vacancy, with adsorption energies at 0.189 eV and 0.236 eV, respectively. This trend suggests that tensile and compressive strain influences the ability of these defective surfaces to bind hydrogen, thus impairing their catalytic efficiency in hydrogenation reactions.

For the Type 2 and Type 3 systems with C vacancies, hydrogen adsorption shows varying sensitivity to strain. In the Type 2 system, adsorption weakens slightly under -3% strain, while in the Type 3 system, strain has an almost negligible effect, with adsorption energies close to the unstrained values. In contrast, the Type 1 system with Ti substitution remains highly stable, with adsorption energies being nearly constant across both tensile and compressive strain conditions.

Electronic Properties and Hydrogen Adsorption The observations from the ELF plots and hydrogen adsorption on pristine and defective systems under unstrained and strained conditions reveal consistent trends in electronic effects. A comparison between pristine and defective systems highlights that the presence of a Mo vacancy leads to significant electronic structure changes at the top surface, which correlates with an increase in hydrogen adsorption energy. This effect remains stable under both tensile and compressive strains. In contrast, for systems with a C vacancy, no significant variations in the ELF plots were observed, regardless of the strain applied, and this holds true for hydrogen adsorption as well. Similarly, in the Type 1 system with Ti substitution, the ELF plots and hydrogen adsorption energies remain nearly unchanged under both strained and unstrained conditions. These results suggest that the changes in spatial distribution of electron pairs, as captured in the ELF plots, have a strong influence on hydrogen adsorption properties. Specifically, the introduction of a Mo vacancy has

a notable impact on adsorption, while C vacancies and Ti substitution cause minimal changes. This indicates that the nature of the defect strongly governs the adsorption behavior, with Mo vacancies resulting in the most significant electronic and catalytic modifications.

Conclusions

Motivated by C-AFM images showing the effect of defects on surface electronics, DFT calculations were performed to investigate the electronic properties of three different types of orthorhombic Mo_2C surfaces. We analyzed the electronic structure using the electron localization function (ELF), projected density of states (PDOS), and hydrogen atom adsorption properties. Comparing pristine and defective Mo_2C systems, we observed that Mo atom vacancies significantly impacted the electronic structure at vacancy sites, primarily due to the disruption of bonding interactions. In contrast, C atom vacancies and Mo substitution with Ti caused minimal changes, aside from reduced ELF values around the Ti atom. Strain effects were also examined, showing that Mo vacancies led to notable changes in the ELF values in the immediate vicinity of the vacancy, while C vacancies and Ti substitution exhibited minimal strain dependence. Considering these changes in the regions associated with electron pairs or bonding sites, a comparative analysis of all types of pristine and defective Mo_2C surfaces was conducted, with a particular focus on hydrogen atom adsorption. The findings indicated that strain can be a powerful tool to modulate catalytic properties on specific orthorhombic Mo_2C surfaces, particularly when combined with defect engineering, providing insights for the design of strain-engineered catalytic materials. Further, the calculations provide a foundational framework for understanding the impact of varying defect concentrations on the properties and behavior of Mo_2C systems. The results also show that careful consideration must be given to both the characteristics of the adsorption site and the applied strain when designing strain-engineered catalytic materials. In summary, these findings provide valuable insights into the impact of defects and strain on the electronic properties and adsorption behavior of Mo_2C surfaces, which could inform the design of more efficient catalysts.

Acknowledgments

The Mo_2C crystals that were studied here via C-AFM were grown by the group of Prof. Goknur Cambaz Buke at TOBB University of Economics and Technology. This work was supported by the Air Force Office of Scientific Research (AFOSR) Award Nos. FA9550-22-1-0358 and

FA9550-22-1-0418.

Author Information

Corresponding information

Ashlie Martini - Department of Mechanical Engineering, University of California Merced, Merced, United States; orcid.org/0000-0003-2017-6081 ; Email: amartini@ucmerced.edu

Authors

Sourabh Kumar - Department of Mechanical Engineering, University of California Merced, Merced, United States; orcid.org/0000-0002-1303-2920; Email: sourabhkumar@ucmerced.edu

Gokay Adabasi - Department of Mechanical Engineering, University of California Merced, Merced, United States; orcid.org/0000-0003-1451-0573; Email: gadabasi@ucmerced.edu

Mehmet Z. Baykara - Department of Mechanical Engineering, University of California Merced, Merced, United States; orcid.org/0000-0002-0278-6022; Email: mehmet.baykara@ucmerced.edu

References

[1] T. Y. Kosolapova, *Carbides: properties, production, and applications*. Springer Science & Business Media, 2012.

[2] L. Toth, *Transition metal carbides and nitrides*. Elsevier, 2014.

[3] K. N. Dinh, Q. Liang, C.-F. Du, J. Zhao, A. I. Y. Tok, H. Mao, and Q. Yan, "Nanostructured metallic transition metal carbides, nitrides, phosphides, and borides for energy storage and conversion," *Nano Today*, vol. 25, pp. 99–121, 2019.

[4] S. A. Rasaki, B. Zhang, K. Anbalgam, T. Thomas, and M. Yang, "Synthesis and application of nano-structured metal nitrides and carbides: A review," *Prog. Solid State Chem.*, vol. 50, pp. 1–15, 2018.

[5] M. Derakhshandeh, M. Eshraghi, and M. Razavi, "Recent developments in the new generation of hard coatings applied on cemented carbide cutting tools," *Int. J. Refract. Met. Hard Mater.*, vol. 111, p. 106077, 2023.

[6] A. Rizzo, S. Goel, M. Luisa Grilli, R. Iglesias, L. Jaworska, V. Lapkovskis, P. Novak, B. O. Postolnyi, and D. Valerini, "The critical raw materials in cutting tools for machining applications: A review," *Materials*, vol. 13, no. 6, p. 1377, 2020.

[7] J. Sun, J. Zhao, Z. Huang, K. Yan, X. Shen, J. Xing, Y. Gao, Y. Jian, H. Yang, and B. Li, "A review on binderless tungsten carbide: development and application," *Nano-Micro Lett.*, vol. 12, pp. 1–37, 2020.

[8] M. Rafique, Q. Fu, J. Han, R. Wang, T. Yao, X. Wang, and B. Song, "Tungsten carbide-based materials for electrocatalytic water splitting: A review," *ChemElectroChem*, vol. 11, no. 6, p. e202300722, 2024.

[9] S. Saha, B. Rajbongshi, V. Ramani, and A. Verma, "Titanium carbide: An emerging electrocatalyst for fuel cell and electrolyser," *Int. J. Hydrogen Energy.*, vol. 46, no. 24, pp. 12801–12821, 2021.

[10] Z. Li and Y. Wu, "2d early transition metal carbides (mxenes) for catalysis," *Small*, vol. 15, no. 29, p. 1804736, 2019.

[11] A. Ul-Hamid, "Microstructure, properties and applications of zr-carbide, zr-nitride and zr-carbonitride coatings: a review," *Mater. Adv.*, vol. 1, no. 5, pp. 1012–1037, 2020.

[12] M. S. A. Sher Shah, G. Y. Jang, K. Zhang, and J. H. Park, "Transition metal carbide-based nanostructures for electrochemical hydrogen and oxygen evolution reactions," *EcoEnergy*, vol. 1, no. 2, pp. 344–374, 2023.

[13] B. Dhandapani, T. S. Clair, and S. Oyama, "Simultaneous hydrodesulfurization, hydrodeoxygenation, and hydrogenation with molybdenum carbide," *Appl. Catal. A: Gen.*, vol. 168, no. 2, pp. 219–228, 1998.

[14] H. Zhou, Z. Chen, E. Kountoupi, A. Tsoukalou, P. M. Abdala, P. Florian, A. Fedorov, and C. R. Müller, "Two-dimensional molybdenum carbide 2d-mo_2c as a superior catalyst for co2 hydrogenation," *Nat. Commun.*, vol. 12, no. 1, p. 5510, 2021.

[15] G. Zhao, K. Rui, S. X. Dou, and W. Sun, "Heterostructures for electrochemical hydrogen evolution reaction: a review," *Adv. Funct. Mater.*, vol. 28, no. 43, p. 1803291, 2018.

[16] J. Wang, Q. Qin, F. Li, Y. Anjarsari, W. Sun, R. Azzahiidah, J. Zou, K. Xiang, H. Ma, J. Jiang, and Arramel, "Recent advances of mxenes mo_2c-based materials for efficient photocatalytic hydrogen evolution reaction," *Carbon Lett.*, vol. 33, no. 5, pp. 1381–1394, 2023.

[17] M. Miao, J. Pan, T. He, Y. Yan, B. Y. Xia, and X. Wang, "Molybdenum carbide-based electrocatalysts for hydrogen evolution reaction," *Chem. Eur. J.*, vol. 23, no. 46, pp. 10947–10961, 2017.

[18] M. Nagai and K. Matsuda, "Low-temperature water–gas shift reaction over cobalt–molybdenum carbide catalyst," *J. Catal.*, vol. 238, no. 2, pp. 489–496, 2006.

[19] J. A. Schaidle, A. C. Lausche, and L. T. Thompson, "Effects of sulfur on mo_2c and pt/mo_2c catalysts: Water gas shift reaction," *J. Catal.*, vol. 272, no. 2, pp. 235–245, 2010.

[20] H. Wang, S. Liu, and K. J. Smith, "Understanding selectivity changes during hydrodesulfurization of dibenzothiophene on mo_2c/carbon catalysts," *J. Catal.*, vol. 369, pp. 427–439, 2019.

[21] P. M. Mortensen, H. W. de Carvalho, J.-D. Grunwaldt, P. A. Jensen, and A. D. Jensen, "Activity and stability of mo_2c/zro_2 as catalyst for hydrodeoxygenation of mixtures of phenol and 1-octanol," *J. Catal.*, vol. 328, pp. 208–215, 2015.

[22] S. Kattel, B. Yan, Y. Yang, J. G. Chen, and P. Liu, "Optimizing binding energies of key intermediates for co2 hydrogenation to methanol over oxide-supported copper," *J. Am. Chem. Soc.*, vol. 138, no. 38, pp. 12440–12450, 2016.

[23] L. Wang, H. Wang, H. Huang, T. Yun, C. Song, and C. Shi, "Transition metal carbides: emerging co2 hydrogenation catalysts, from recent advance to future exploration," *Adv. Funct. Mater.*, vol. 34, no. 7, p. 2309850, 2024.

[24] L. Meng, E. V. Pokochueva, Z. Chen, A. Fedorov, F. Viñes, F. Illas, and I. V. Koptyug, "Contrasting metallic (rh0) and carbidic (2d-mo2c mxene) surfaces in olefin hydrogenation provides insights on the origin of the pairwise hydrogen addition," *ACS Catal.*, vol. 14, no. 16, pp. 12500–12511, 2024.

[25] N. M. Schweitzer, J. A. Schaidle, O. K. Ezekoye, X. Pan, S. Linic, and L. T. Thompson, "High activity carbide supported catalysts for water gas shift," *J. Am. Chem. Soc.*, vol. 133, no. 8, pp. 2378–2381, 2011.

[26] R. A. Mir, S. Upadhyay, and O. Pandey, "A review on recent advances and progress in mo_2c@ c: a suitable and stable electrocatalyst for her," *Int. J. Hydrogen Energy.*, vol. 48, no. 35, pp. 13044–13067, 2023.

[27] K. M. Reddy, T. Rao, J. Revathi, and J. Joardar, "Structural stability of α/β-mo_2c during thermochemical processing," *J. Alloys Compd.*, vol. 494, no. 1-2, pp. 386–391, 2010.

[28] K. Page, J. Li, R. Savinelli, H. N. Szumila, J. Zhang, J. K. Stalick, T. Proffen, S. L. Scott, and R. Seshadri, "Reciprocal-space and real-space neutron investigation of nanostructured mo_2c and wc," *Solid State Sci.*, vol. 10, no. 11, pp. 1499–1510, 2008.

[29] J. Haines, J. Léger, C. Chateau, and J. Lowther, "Experimental and theoretical investigation of mo_2c at high pressure," *J. Condens. Matter Phys.*, vol. 13, no. 11, p. 2447, 2001.

[30] A. Vojvodic, "Steam reforming on transition-metal carbides from density-functional theory," *Catal. Lett.*, vol. 142, pp. 728–735, 2012.

[31] M. Cankurtaran, S. Dodd, and B. James, "Ultrasonic study of the temperature and pressure dependences of the elastic properties of ceramic dimolybdenum carbide (α-mo_2c)," *J. Mater. Sci.*, vol. 39, pp. 1241–1248, 2004.

[32] M. Naher and S. Naqib, "Possible applications of mo_2c in the orthorhombic and hexagonal phases explored via ab-initio investigations of elastic, bonding, optoelectronic and thermophysical properties," *Results Phys.*, vol. 37, p. 105505, 2022.

[33] Á. Morales-García, J. He, P. Lyu, and P. Nachtigall, "Exploring the stability and reactivity of ni 2 p and mo 2 c catalysts using ab initio atomistic thermodynamics and conceptual dft approaches," *Biomass. Convers. Biorefin.*, vol. 7, pp. 377–383, 2017.

[34] P. Liu, J. A. Rodriguez, T. Asakura, J. Gomes, and K. Nakamura, "Desulfurization reactions on ni_2p (001) and α-mo_2c (001) surfaces: complex role of p and c sites," *J. Phys. Chem. B.*, vol. 109, no. 10, pp. 4575–4583, 2005.

[35] F. Zhang, L. He, S. Lian, M. Wang, X. Chen, J. Yin, H. Pan, J. Ren, and M. Chen, "Investigation of strain and transition-metal doping effect on hydrogen evolution reaction catalysts of mo_2c, mop, and ni_2p," *J. Phys. Chem. C*, vol. 125, no. 35, pp. 19119–19130, 2021.

[36] Y. Fan, C. Xu, X. Liu, C. Ma, Y. Yin, H.-M. Cheng, W. Ren, and X. Li, "Distinct superconducting properties and hydrostatic pressure effects in 2d α-and β-mo2c crystal sheets," *NPG Asia Mater*, vol. 12, no. 1, p. 60, 2020.

[37] S. A. Sumaiya, I. Demiroglu, O. R. Caylan, G. C. Buke, C. Sevik, and M. Z. Baykara, "Atomically resolved defects on thin molybdenum carbide (α-mo_2c) crystals," *Langmuir*, vol. 39, no. 31, pp. 10788–10794, 2023.

[38] C. de Oliveira, D. R. Salahub, H. A. de Abreu, and H. A. Duarte, "Native defects in α-mo_2c: insights from first-principles calculations," *J. Phys. Chem. C*, vol. 118, no. 44, pp. 25517–25524, 2014.

[39] X. Cao, H. Bai, W. Wu, H. Bao, and Y. Li, "Improving the catalytic activity of two-dimensional mo_2c for hydrogen evolution reaction by doping and vacancy defects," *Int. J. Hydrogen Energy.*, vol. 47, no. 91, pp. 38517–38523, 2022.

[40] T. Wang, Y.-W. Li, J. Wang, M. Beller, and H. Jiao, "Dissociative hydrogen adsorption on the hexagonal mo_2c phase at high coverage," *J. Phys. Chem. C*, vol. 118, no. 15, pp. 8079–8089, 2014.

[41] L. Yang, H. Chen, F. Jia, W. Peng, X. Tian, L. Xia, X. Wu, and S. Song, "Emerging hexagonal mo_2c nanosheet with (002) facet exposure and cu incorporation for peroxymonosulfate activation toward antibiotic degradation," *ACS Appl. Mater. Interfaces.*, vol. 13, no. 12, pp. 14342–14354, 2021.

[42] B. Zhang, J. Zhou, S. R. Elliott, and Z. Sun, "Two-dimensional molybdenum carbides: active electrocatalysts for the nitrogen reduction reaction," *J. Mater. Chem. A*, vol. 8, no. 45, pp. 23947–23954, 2020.

[43] H. Lou, T. Yu, J. Ma, S. Zhang, A. Bergara, and G. Yang, "Achieving high hydrogen evolution reaction activity of a mo_2c monolayer," *Phys. Chem. Chem. Phys.*, vol. 22, no. 45, pp. 26189–26199, 2020.

[44] P. Giannozzi, S. Baroni, N. Bonini, M. Calandra, R. Car, C. Cavazzoni, D. Ceresoli, G. L. Chiarotti, M. Cococcioni, I. Dabo, A. Dal Corso, S. de Gironcoli, S. Fabris, G. Fratesi, R. Gebauer, U. Gerstmann, C. Gougoussis, A. Kokalj, M. Lazzeri, L. Martin-Samos, N. Marzari, F. Mauri, R. Mazzarello, S. Paolini, A. Pasquarello, L. Paulatto, C. Sbraccia, S. Scandolo, G. Sclauzero, A. P. Seitsonen, A. Smogunov, P. Umari, and R. M. Wentzcovitch, "Quantum espresso: a modular and open-source software project for quantum simulations of materials," *J. Phys.: Condens. Matter*, vol. 21, no. 39, p. 395502 (19pp), 2009.

[45] P. Giannozzi, O. Andreussi, T. Brumme, O. Bunau, M. B. Nardelli, M. Calandra, R. Car, C. Cavazzoni, D. Ceresoli, M. Cococcioni, N. Colonna, I. Carnimeo, A. D. Corso, S. de Gironcoli, P. Delugas, R. A. D. Jr, A. Ferretti, A. Floris, G. Fratesi, G. Fugallo, R. Gebauer, U. Gerstmann, F. Giustino, T. Gorni, J. Jia, M. Kawamura, H.-Y. Ko, A. Kokalj, E. Küçükbenli, M. Lazzeri, M. Marsili, N. Marzari, F. Mauri, N. L. Nguyen, H.-V. Nguyen, A. O. de-la Roza, L. Paulatto, S. Poncé, D. Rocca, R. Sabatini, B. Santra, M. Schlipf, A. P. Seitsonen, A. Smogunov, I. Timrov, T. Thonhauser, P. Umari, N. Vast, X. Wu, and S. Baroni, "Advanced capabilities for materials modelling with quantum espresso," *J. Phys.: Condens. Matter*, vol. 29, no. 46, p. 465901, 2017.

[46] A. N. Christensen, "A neutron diffraction investigation on a crystal of alpha-mo2c.," 1977.

[47] J. P. Perdew, K. Burke, and M. Ernzerhof, "Generalized gradient approximation made simple," *Phys. Rev. Lett.*, vol. 77, no. 18, p. 3865, 1996.

[48] G. C. Buke, O. R. Caylan, and O. T. Ogurtani, "Growth mechanism of 2d mo2c on cu via cvd," *Cryst. Growth Des.*, vol. 23, no. 8, pp. 5462–5468, 2023.

[49] J. E. Sader, J. W. Chon, and P. Mulvaney, "Calibration of rectangular atomic force microscope cantilevers," *Rev. Sci. Instrum.*, vol. 70, no. 10, pp. 3967–3969, 1999.

[50] S. A. Sumaiya, J. Liu, and M. Z. Baykara, "True atomic-resolution surface imaging and manipulation under ambient conditions via conductive atomic force microscopy," *ACS nano*, vol. 16, no. 12, pp. 20086–20093, 2022.

[51] A. D. Becke and K. E. Edgecombe, "A simple measure of electron localization in atomic and molecular systems," *J.Chem. Phys.*, vol. 92, no. 9, pp. 5397–5403, 1990.

[52] A. Savin, R. Nesper, S. Wengert, and T. F. Fässler, "Elf: The electron localization function," *Angew. Chem., Int. Ed. Engl.*, vol. 36, no. 17, pp. 1808–1832, 1997.

[53] T. Wang, X. Tian, Y. Yang, Y.-W. Li, J. Wang, M. Beller, and H. Jiao, "Surface morphology of orthorhombic mo_2c catalyst and high coverage hydrogen adsorption," *Surf. Sci.*, vol. 651, pp. 195–202, 2016.

[54] S. Posada-Pérez, F. Viñes, R. Valero, J. A. Rodriguez, and F. Illas, "Adsorption and dissociation of molecular hydrogen on orthorhombic β-mo_2c and cubic δ-moc (001) surfaces," *Surf. Sci.*, vol. 656, pp. 24–32, 2017.

TOC Graphic